

Thickness-Controlled Phase Transitions of AB Diblock Copolymers in Asymmetric Ultrathin Films

Luyang Li, Xiangmeng Jia, Qingshu Dong, Jiajia Zhou,* and Weihua Li*



Cite This: *Macromolecules* 2023, 56, 5932–5940



Read Online

ACCESS |



Metrics & More

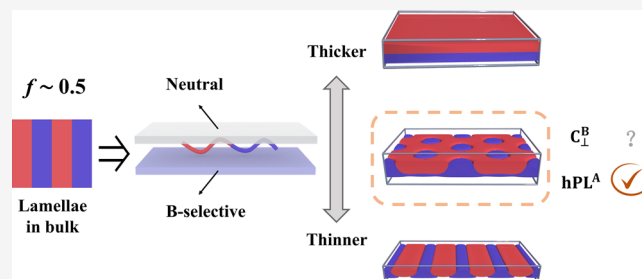


Article Recommendations



Supporting Information

ABSTRACT: An unusual hexagonal dot pattern has been observed in thin films of symmetric diblock copolymers experimentally. In order to verify the stability of the hexagonal dot pattern and understand its formation mechanism, we investigate the self-assembly of AB diblock copolymers in ultrathin films with a neutral top surface and a B-selective bottom surface using self-consistent field theory (SCFT) and dissipative particle dynamics (DPD). Our SCFT results reveal that ideally symmetric diblock copolymers with A-block volume fraction $f = 0.5$ can indeed form a hexagonal dot pattern in a certain range of film thickness (h), which is actually a half-period perforated lamellar (hPL^A) morphology. The hPL^A morphology transfers to a patternless half-period parallel lamella ($hL_{||}$) with increasing h and to a stripe pattern (L_{\perp}) with decreasing h . The phase diagram with respect to f and h further demonstrates that the stable region of hPL^A shifts to small f as h increases and disappears at a critical value of h . The formation of the hPL^A region is mainly caused by the competition between the A/B interfacial energy and the overall surface energy (including top and bottom). In addition, the formation of hPL^A is also verified by DPD simulations. Therefore, our work confirms that the experimentally observed dot pattern in thin films of symmetric diblock copolymers is an equilibrium morphology, the formation of which requires ultrathin thickness and asymmetric surface affinities.



INTRODUCTION

Connecting chemically incompatible polymers by a covalent bond gives rise to the block copolymers (BCPs), which are important in the family of polymeric materials. Due to the chemical immiscibility and the permanent bonding, different blocks spontaneously segregate to form periodic structures at the macromolecular length scale (typically a few to a few hundred nanometers),^{1–3} which is useful for applications such as photonic crystals,^{4,5} semiconductor materials,^{6,7} solar cells,⁸ etc. Previous studies have shown that for linear diblock copolymers, the bulk phase behavior is influenced by several factors, such as the composition (volume fraction of one component, f),⁹ the degree of polymerization (N),¹⁰ the segment length (b),¹¹ and Flory–Huggins interaction parameter (χ)¹² that characterizes the degree of incompatibility. Among these parameters, the volume fraction f has a significant effect on the phase behavior, that is, as f increases from asymmetric to symmetric ($f = 0.5$), the thermodynamically stable phases are spheres, cylinders, bicontinuous networks, and lamellae in sequence.^{9,13} In many practical applications, the BCP materials are often prepared as thin films via spin-coating and then subsequently processed.¹⁴ In such films, BCP self-assembly is also sensitive to some external conditions, such as the surface boundaries.^{15,16} Since the feature size of these nanostructures ranges from hundreds of down to a few nanometers, the self-assembly of BCPs provides a possibility of pushing semi-

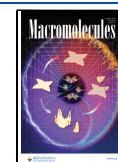
conductor technology and nanophotonics to finer precision.^{17–20} In fact, the directed self-assembly (DSA) of BCP thin films, which combines the technology of the traditional lithography and the spontaneous formation of nanostructures by BCPs, has been regarded as one of the most promising next-generation lithography techniques.^{6,7,21}

For AB diblock copolymers in the bulk, the self-assembly behavior has been intensively studied both experimentally^{22,23} and theoretically^{3,9} and are considered well-understood. However, their self-assembly behavior in thin films is more complicated^{24–26} and the understanding of them is far from complete due to the additional variables including the film thickness (h) and surface affinity. These two factors are relatively easy to control and often used to regulate the film morphology.^{27–31} Film thickness, controlled by the spin rate, defines the dimension between two confining boundaries that breaks the translational symmetry of the periodic structures in the direction normal to the substrate. Thus, h is the dominant

Received: April 13, 2023

Revised: June 17, 2023

Published: July 19, 2023



factor dictating domain arrangement in the direction perpendicular to the substrate.³² Besides the spatial constraint, the top and bottom surfaces introduce additional interactions with each BCP component, which are defined as surface affinities. The surface affinities impact the assembled morphologies by affecting the geometrical shape and the orientation of the domains.^{16,26,29,31,33}

Since the surface-induced ordering of diblock copolymer films was first observed by Anastasiadis et al.,¹⁵ the phase behavior of BCP thin films has attracted intensive interest.^{16,34–37} When a symmetric AB diblock copolymer is confined between two surfaces that are preferential to one block at a thickness h that is integer multiples of its bulk period, L_0 , parallel lamellae are stably formed where the preferred block wets the two surfaces. But, if h deviates from integer multiples of L_0 , there are usually two modes to mitigate the mismatching. One is that the film deforms into “islands and holes”,^{36,38} allowing the coexistence of k and $k + 1$ (k is integer) periods of lamellae oriented parallel to the substrate, which is common for the deformable surfaces, such as the BCP–air interface. The other is to form parallel lamellar morphology (L_{\parallel}) with a period that deviates from L_0 and is adjusted according to h , which is preferred by the BCP films sandwiched between two parallel slabs.^{24,28} With the non-deformable surfaces, an energy penalty results from the overstretching of the chains or the increase of the area of the A/B interface when the period is adjusted to deviate severely from L_0 .²⁴ In contrast, the perpendicular lamellar morphology (L_{\perp}) can adjust its period freely and tends to form in thin films whose thicknesses are noninteger multiples of L_0 .³² However, both components in the perpendicular morphology must be in contact with both surfaces of the film, leading to unfavorable interaction energy between the selective surface and the disfavored component. Usually, the competition between the period commensurability and the surface affinities in symmetric thin films dictates the formation of the parallel or perpendicular morphology.^{16,26}

The self-assembly behavior is more complicated in asymmetric thin films than that in symmetric films^{39–44} and thus is less understood. Very recently, Shenhar et al.⁴⁵ studied the self-assembly of a near-symmetric PS-*b*-PMMA diblock copolymer melt ($f_{\text{PS}} = 0.48$) in asymmetric ultrathin films overlaid on a topographically patterned substrate with a neutral top surface and a PMMA-selective substrate. Interestingly, the lamella-forming block copolymer film deposited on the plateaus gave rise to a morphology whose top view is a hexagonal “dot” pattern. This behavior was attributed to the local film thickness, the asymmetric surface affinities, and the topographical substrate.^{46,47} Nevertheless, the formation mechanism of the hexagonal dot pattern by the lamella-forming block copolymer needs to be further elucidated theoretically.

The neutral top surface enables the vertical orientation of domains, while the selective bottom surface tends to attract the preferred component.^{25,48} Accordingly, we may assume that a mixed morphology composed of both parallel and vertically oriented domains may form in this situation. In 1997, Matsen proposed one class of mixed morphologies with lamellae parallel and perpendicular to the two surfaces, respectively.¹⁶ One of them contains a wetting layer on only one surface, which is referred to as L_{M}^1 . On the one hand, his self-consistent field theory (SCFT) results demonstrated that the L_{M}^1 phase remains metastable throughout the varying thickness for $f = 0.5$ in neutral-selective films. On the other hand, the top view of the L_{M}^1 morphology looks like stripes, differing from the hexagonal dots

observed by Shenhar et al.⁴⁵ In fact, the dot morphology was also observed in the thin film of symmetric diblock copolymers in earlier experiments by Fasolka and Mayes.⁴⁰ They used two-dimensional (2D) SCFT calculations to rationalize the formation of the dots, but the 2D calculations cannot distinguish the dot pattern from the stripe pattern because of their similar cross sections normal to the surfaces.⁴⁹ Accordingly, they referred to the stripe pattern as a “hybrid” lamellar structure (HY). In 2010, Meng and Wang⁴² carried out a systematic SCFT study in three dimensions (3D) to examine the formation of mixed morphologies in asymmetric films. They predicted a stable hexagonally arranged dot pattern formed by symmetric diblock copolymers, which they denoted as $T_1(3D)$, and regarded both this morphology and its 2D counterpart, $T_1(2D)$, as arising from a combination of a wetting layer on the substrate and an HY layer on the top surface. Although the $T_1(3D)$ morphology exhibited a hexagonal lattice of dots on the top, it contains one more layer of polymer chains than the experimental morphology of Shenhar et al.⁴⁵ In other words, the component that wets the substrate does not form the hexagonal dots on the top surface in $T_1(3D)$, while the bottom wetting layer and the top hexagonal dots consist of the same component in the observed results of Fasolka et al.^{40,49} and Shenhar et al.⁴⁵ Therefore, the experimental dot morphology should be formed in films thinner than $T_1(3D)$.

Based on the above discussions, we turn our attention to the phase behavior of AB diblock copolymer thin films confined between a neutral top surface and a B-selective substrate. According to previous experimental^{40,45} and theoretical²⁶ studies, we assume a series of possible candidate morphologies. Then, we use SCFT coupled with the masking scheme to study the thermodynamic stability of these candidate morphologies, focusing on the impact of the film thickness and the interaction strength of the bottom surface on the formation of these different morphologies, especially the hexagonal dot pattern. Additionally, the kinetic stability of these structures is verified through dissipative particle dynamics (DPD). We are inspired to explore the characteristics of the dot morphology that has been observed in experiments but not yet been fully explained theoretically and to reveal its formation mechanism.

THEORY AND METHODS

Self-Consistent Field Theory (SCFT). We consider an incompressible melt of volume V composed of n identical AB diblock copolymer chains, which are confined between two impenetrable plates separated by a distance of h . For simplicity, we assume that the two different blocks have equal segment length b and density ρ_0 . The total number of the segments on each diblock copolymer chain is specified as N , and the numbers of A-segments and B-segments are denoted by fN and $(1 - f)N$, respectively, where f is the volume fraction of block A. The immiscibility between A- and B-blocks is characterized by the product $\chi_{\text{AB}}N$. In the confined system, periodic boundary conditions are used on the lateral x - and y -directions, while the masking scheme⁵⁰ are used to model the attenuation of the segment density near the surface on the normal z -direction. In the masking scheme, the density of the segments at the surface is defined as 0, and it continuously increases to 1 from the surface toward the inside of the film. Two wall components, the top (T) and the bottom (W), are introduced as the boundary conditions (Figure 1a), which remain unchanged during SCFT iterations. The density distribution of the wall components are given by the following expressions

$$\phi_T(r) = \begin{cases} 1 & \text{for } h + D_0 \\ & \leq r_z \\ & \leq h + 2D_0 \\ \frac{1}{2} \{1 - \tanh[(h + D_0 - r_z - \sigma)/\lambda]\} & \text{for } h + D_0 - 2\sigma \\ & \leq r_z \\ & \leq D_0 + h \\ 0 & \text{otherwise} \end{cases} \quad (1)$$

$$\phi_W(r) = \begin{cases} 1 & \text{for } 0 \leq r_z \leq D_0 \\ \frac{1}{2} \{1 - \tanh[(r_z - D_0 - \sigma)/\lambda]\} & \text{for } D_0 \leq r_z \leq D_0 + 2\sigma \\ 0 & \text{otherwise} \end{cases} \quad (2)$$

where D_0 denotes the thickness of the two impenetrable walls, and σ and λ determine the width and shape of the wall interface, respectively. We fix $D_0 = 0.20R_g$, $\sigma = 0.50R_g$, and $\lambda = 0.15R_g$, where $R_g = N^{1/2}b/\sqrt{6}$ is the radius of gyration of an unperturbed polymer chain with N statistical segments.

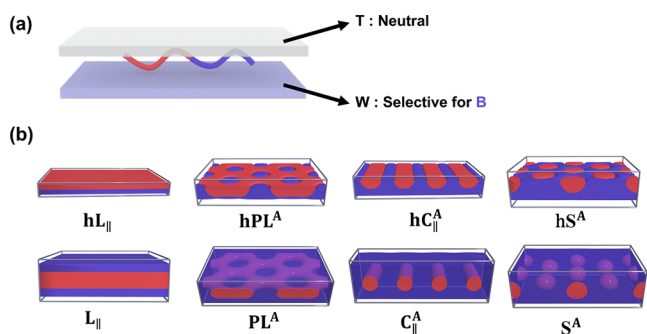


Figure 1. (a) Schematic of an AB diblock copolymer ultrathin film with a neutral top surface and a B-selective bottom surface. (b) Candidate morphologies including monolayer or half-period ones (top row) and their corresponding double-layer or full-period ones (bottom row). The A- and B-blocks and their corresponding domains are represented in red and blue colors, respectively.

The wetting preference to A- and B-components is realized by the interaction parameters between them and the wall components, $\chi_{ij}N$ ($i = A/B$ and $j = T/W$). The affinities of the top and bottom surfaces were set as $\chi_{AW}N = -\chi_{BW}N = 35$ and $\chi_{AT}N = \chi_{BT}N = 0$ to simulate a B-preferential substrate and a nonpreferential interaction between the blocks and the top wall. With the introduced wall components, the free energy functional of SCFT on the basis of Gaussian chain model at a given temperature T_0 is written as

$$\begin{aligned} \frac{F}{nk_B T_0} = & -\ln Q + \frac{1}{V} \int_{D_0 \leq r_z \leq D_0+h} d\mathbf{r} \{ \chi_{AB} N \phi_A(\mathbf{r}) \phi_B(\mathbf{r}) \\ & + \chi_{AW} N \phi_A(\mathbf{r}) \phi_W(\mathbf{r}) + \chi_{BW} N \phi_B(\mathbf{r}) \phi_W(\mathbf{r}) \\ & + \chi_{AT} N \phi_A(\mathbf{r}) \phi_T(\mathbf{r}) + \chi_{BT} N \phi_B(\mathbf{r}) \phi_T(\mathbf{r}) - w_A \phi_A(\mathbf{r}) \\ & - w_B \phi_B(\mathbf{r}) - \xi(\mathbf{r}) [1 - \phi_A(\mathbf{r}) - \phi_B(\mathbf{r}) - \phi_W(\mathbf{r}) \\ & - \phi_T(\mathbf{r})] \} \end{aligned} \quad (3)$$

where k_B is the Boltzmann constant, $\phi_A(\mathbf{r})$ and $\phi_B(\mathbf{r})$ are the spatial local volume fractions of A- and B-blocks at \mathbf{r} , while $w_A(\mathbf{r})$ and $w_B(\mathbf{r})$ are their potential fields, respectively, $\eta(\mathbf{r})$ is a Lagrange multiplier used to enforce the incompressibility condition, $\phi_A(\mathbf{r}) + \phi_B(\mathbf{r}) + \phi_T(\mathbf{r}) + \phi_W(\mathbf{r}) = 1$, and the quantity Q is the partition function of a single copolymer

chain interacting with its mean fields. Other details of the SCFT can be found in the Supporting Information (SI).

Dissipative Particle Dynamics (DPD). DPD simulations are performed in the NVT canonical ensemble. The description of the standard methods is given in the SI. To ensure sufficient accuracy for describing the ordered morphologies formed in ultrathin films, we choose a relative large number of beads for each copolymer chain, e.g., 40.

The Lennard-Jones (LJ) potential is utilized to describe the interaction between the walls and beads⁵¹

$$U(r) = 4\epsilon \left[\left(\frac{\sigma}{r} \right)^{12} - \left(\frac{\sigma}{r} \right)^6 \right] \quad (4)$$

where r is the bead–wall distance, ϵ is the depth of the potential well, and σ is set to be 1. The two walls are set at $r_z = 0$ and $r_z = h + 0.7$, perpendicular to the z -direction, where 0.7 is used to compensate the reduction in film thickness caused by the repulsion of the beads from the walls. In the simulation, r_{cut} is the cutoff distance where the interactions are truncated. Usually, $r_{\text{cut}} = 2^{1/6}$ means strong repulsion and $r_{\text{cut}} = 1.5$ means weak attraction. The parameter $\Gamma_{ij} = (\epsilon, r_{\text{cut}})$ describes the affinities of the two surfaces (i and j represent the component and the surface, respectively), that is, $\Gamma_{A,W} = (1, 2^{1/6})$, $\Gamma_{B,W} = (2, 1.5)$, and $\Gamma_{A,T} = \Gamma_{B,T} = (1, 1.5)$.

The surface attraction is realized by the selective interaction of the wall component to the two different blocks in the masking model of SCFT, while it is acted by the LJ potential in DPD simulation. It may be challenging to obtain a quantitative matching for the surface attraction. In our work, we mainly focus on the formation mechanism of these different ordered morphologies in lamella-forming diblock copolymer thin films. Therefore, we do not do a quantitative matching of the surface attraction between the DPD model and SCFT.

Our simulations are performed with the HOOMD-blue (version 2.9.7) simulation package, which was developed and maintained by Anderson et al.⁵² In this study, the simulation box size is set to be $50 \times 50 \times r_z (R_g^3)$, where $R_g \approx 3.0$ is the average radius of gyration of an unperturbed polymer chain with 40 beads. $N_b = 40$ represents the total number of beads in a single chain, and $a_{AB} = 27.45$ characterizes the interaction parameter between A- and B-particles. The integrating time step Δt is set to be 0.01 to achieve a balance between simulation stability and performance, and the total number of simulation steps is set to be 10^7 . Three parallel samples are run for each set of parameters. All of the samples are initialized from a disordered state and considered to have reached the equilibrium state if the morphologies remain stable for more than 3×10^6 steps.

RESULTS AND DISCUSSION

Since the neutral top surface has no preference for either block while the substrate is strongly selective to the B-block, as illustrated in Figure 1a, it is reasonable to consider one layer of “standing” copolymer chains to form the parallel lamellar morphology of half-period (denoted as hL_{\parallel}) with a wetting B-layer on the bottom surface as a candidate phase. As decreasing the volume fraction f gradually from symmetric composition, the top pattern of A-domains of the half-period morphology changes under the hard confinement of the neutral top surface from a complete layer to a network, stripes, and dots,⁵³ which correspond to a half perforated lamella (hPL^A), semicylinders (hC_{\parallel}^A), and hemispheres (hS^A), respectively (depicted in Figure 1b, top row). When the film thickness is doubled, the corresponding bilayer (or full-period) morphologies can be produced by superimposing the mirror-symmetric counterparts of the monolayers with respect to the top surface on top of themselves, denoted as L_{\parallel} , PL^A , C_{\parallel}^A , and S^A , respectively (depicted in Figure 1b, bottom row). When the film thickness deviates from half-period or one period, the system will adopt a morphology from the ones illustrated in Figure 1b according to

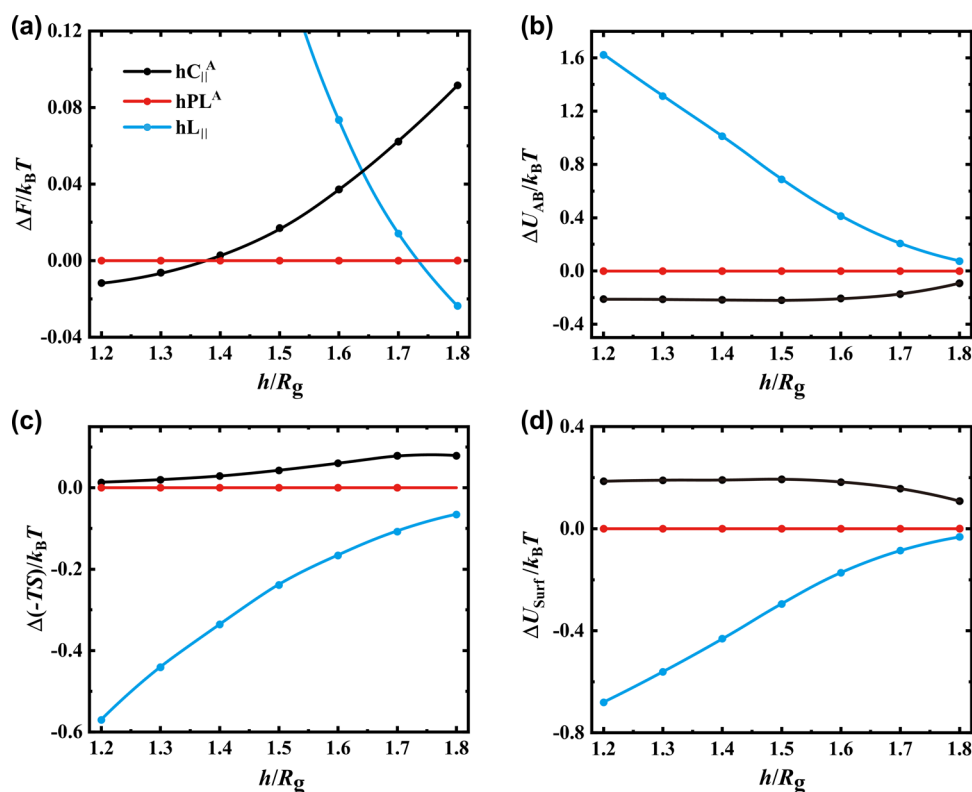


Figure 2. Comparisons of (a) free energy, (b) A/B interfacial energy, (c) entropic contribution, and (d) surface energy with increasing h for $f = 0.5$, $\chi_{AB}N = 30$, $\chi_{AW}N = -\chi_{BW}N = 35$, and $\chi_{AT}N = \chi_{BT}N = 0$.

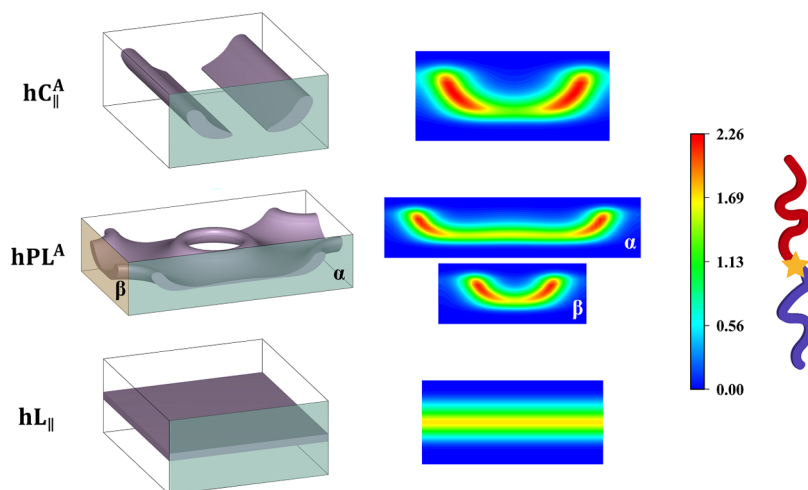


Figure 3. Isosurface plots (left) and their respective typical cross-sectional profiles (right) of the distribution of the junction point (marked with an orange star) in the $hC_{||}^A$, hPL^A , and $hL_{||}$ morphologies for $f = 0.5$ at $h = 1.6R_g$.

the BCP composition and accommodate to the mismatched thickness by adjusting the stretching and packing of chains.

It is worth noting that the hPL^A morphology viewed from above exhibits a hexagonal array of B-dots, exactly corresponding to the morphology observed in the experiments.^{40,45} To demonstrate whether the hPL^A morphology is thermodynamically stable in the asymmetric ultrathin film of symmetric AB diblock copolymers, we first calculate and compare the free energy of $hC_{||}^A$, hPL^A , and $hL_{||}$ for varying film thicknesses h (Figure 2a). As expected, the stable morphology is $hL_{||}$ when h is around half the lamellar period ($L_0/2 = 2.23R_g$). As h decreases, the $hL_{||}$ morphology changes to hPL^A at $h \approx 1.73R_g$ and then to

$hC_{||}^A$ at $h \approx 1.38R_g$. Therefore, our SCFT result verifies that the hPL^A morphology has a stability window within $1.38 < h < 1.73$, confirming that the hexagonal array of dots experimentally formed by the lamella-forming diblock copolymers should be an equilibrium morphology. Note that the $hC_{||}^A$ morphology looks like stripes from above, similar to asymmetric perpendicular lamellae (L_{\perp}), especially in the ultrathin films.

To analyze the transition mechanisms, we separate the free energy into its components, namely, the interfacial energy (ΔU_{AB}), the entropic contribution ($\Delta(-TS)$), and the surface energy (ΔU_{Surf}). As shown in Figure 2b, the A/B interfacial energy of $hL_{||}$ increases quickly compared to hPL^A with

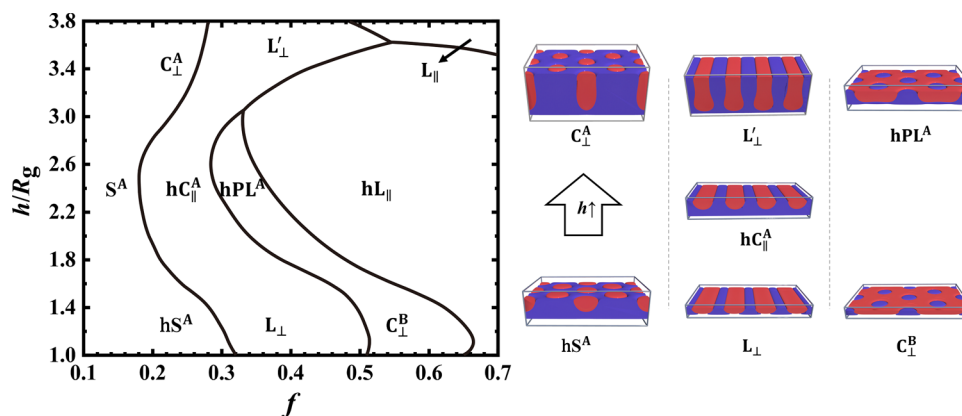


Figure 4. Phase diagram with respect to f and h for $\chi_{AB}N = 30$, $\chi_{AW}N = -\chi_{BW}N = 35$, and $\chi_{AT}N = \chi_{BT}N = 0$ (left), and three continuous morphological transitions with increasing h (right), which are $hS^A \rightarrow C_{\perp}^A$, $L_{\perp} \rightarrow hC_{||}^A \rightarrow L_{\perp}^A$, and $C_{\perp}^B \rightarrow hPL^A$.

decreasing h . In the $hL_{||}$ morphology, the copolymer chains are oriented perpendicular to the confining surfaces and extend from the top to the bottom in the gap between them. For a perpendicularly oriented chain, its extension is roughly proportional to h , and its interfacial area is proportional to h^{-1} because of its conserved volume. Accordingly, the magnitude of the attractive energy of the bottom surface to B-block decreases with increasing h . Moreover, the decreased extension of the chain lowers the entropic contribution to the energy of the system. In the $hC_{||}^A$ (or L_{\perp}) morphology, most of the copolymer chains orient parallel to the surfaces, and the hPL^A morphology is an intermediate between the $hL_{||}$ and $hC_{||}^A$. In striking contrast to the limit imposed on the extension of the perpendicularly oriented chain by the film thickness, the parallel-oriented chain can adjust its extension in the parallel plane regardless of the thickness. As a consequence, the addition of the parallel chains with decreasing film thickness lowers the interfacial energy while raising the entropic contribution (see Figure 2b,c). At the same time, the parallel packing of the copolymer chains also reduces the contact between the B-block and the bottom surface, leading to higher surface energy (Figure 2d). Since the stretching energy of the perpendicular chain is approximately proportional to $h^{2,3}$, the decrease in that cannot offset the increase in interfacial energy as h decreases. Additionally, the interaction width of the surface potential in the masking method is narrower than the A/B interfacial width, so the gain in the surface energy is much less than the penalty of the interfacial energy. This is why $hL_{||}$ transfers to hPL^A and then to $hC_{||}^A$ as h decreases.

To confirm the transition mechanism discussed above, we plot the distribution of the junction point for $hL_{||}$, hPL^A , and $hC_{||}^A$ at $h = 1.6R_g$ as shown in Figure 3. In the $hL_{||}$ morphology, the junction point has a parallel layering distribution in the center of the film, confirming that most of diblock chains are mainly aligned along the normal direction. In contrast, the aggregating regions in the $hC_{||}^A$ tend to be perpendicular to the surfaces; however, they are significantly tilted by the B-selective bottom surface. Such a distribution indicates that a large portion of chains are aligned parallel with the surfaces, whereas a small portion of chains are normal to lower the surface energy. The distribution of the junction point in hPL^A can be seen as the mixture of the two cases of $hL_{||}$ and $hC_{||}^A$.

The above discussions have confirmed that the hexagonal dot pattern observed in the experiments is the half-period perforated lamellar morphology (hPL^A), and it can be formed by the ideally symmetric diblock copolymer in ultrathin films. To demonstrate

how the formation of this morphology will be influenced by the volume fraction f and the thickness h , we construct a two-dimensional phase diagram with respect to f and h for $\chi_{AB}N = 30$ (Figure 4). This phase diagram suggests that the stable region of hPL^A ranges from $f \approx 0.28$ to $f \approx 0.66$ with varying h . Overall, the phase region shifts to small f with increasing h , but it disappears when $h \gtrsim 3.0R_g$. Consequently, $hC_{||}^A$ transfers directly to $hL_{||}$ for $3.0R_g < h < 3.6R_g$. In the considered range of h , the phase behavior of the diblock copolymers deviates significantly from that in the bulk. These deviations can be attributed to the strong confinement effect arising from the small confining size, which is smaller than or comparable to the bulk period of the copolymer.⁵⁴ Moreover, the strong affinity between the B-block and the bottom surface plays a crucial role. Masten and Griffiths⁵⁵ have studied the self-assembly of grafted diblock copolymers, and they predicted some similar ordered morphologies, such as hex₁ (hPL^A), stripe ($hC_{||}^A$), and hex (hS^A). In the grafted system, the phase transitions are mainly tuned by the composition. In contrast, for the nontethered ideally symmetric diblock copolymers, the formation of these morphologies is mainly controlled by the film thickness and the asymmetric affinities.

It is worth mentioning that the geometry of these domains changes continuously with h . For example, hPL^A changes to what is like perpendicularly standing B-cylinders (i.e., C_{\perp}^B) at very small h . This is because the amount of perpendicularly aligned chains that diminish the surface energy is largely suppressed, leading to very little amount of B-blocks attracted to the bottom surface. To lower the surface energy, the “B-cylinders” become “mountain-like” in shape.⁵⁶ Nevertheless, these B-domains have a positive curvature, and thus, a low volume fraction of B-block or large f favors its formation. Similarly, the $hC_{||}^A$ morphology changes to be like perpendicular lamellae (L_{\perp}) as h decreases. Though the B-domain in the L_{\perp} morphology also looks like an ellipsoidal cylinder, its curvature is still lower than that of the perpendicular “B-cylinders” in C_{\perp}^B . This is why the transition from $hC_{||}^A$ to hPL^A is shifted to large f ($0.5 < f < 0.66$) for $1.0R_g < h < 1.4R_g$.

One period PL^A morphology is often formed by the gyroid-forming diblock copolymers in symmetric thin films with proper thickness, locating between the parallel cylinder and lamellar morphologies with varying f .²⁶ In the asymmetric thin films, the transition sequence of $hC_{||}^A/L_{\perp} \rightarrow hPL^A \rightarrow hL_{||}$ is analogy to that of one period morphologies. In the previous work by Li et al.,²⁶ the PL^A morphology was observed in a smaller range of thickness

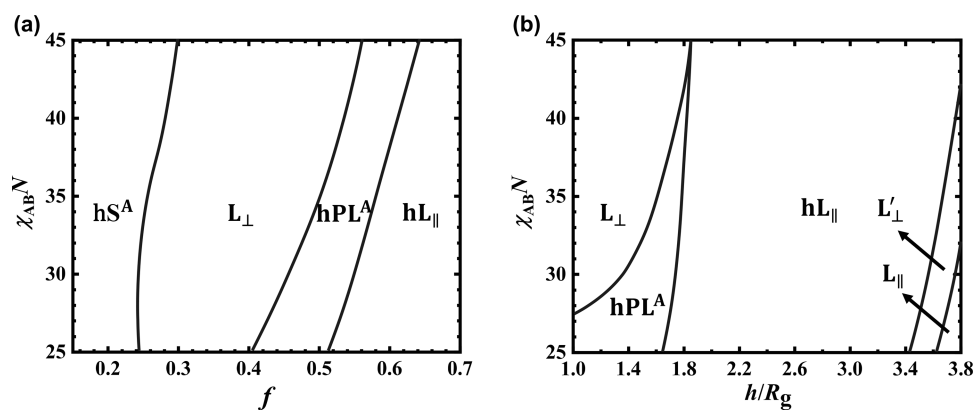


Figure 5. Phase diagrams of (a) $\chi_{AB}N - f$ at $h = 1.6R_g$ and (b) $\chi_{AB}N - h$ for $f = 0.5$.

than its competing cylinder and lamellar morphologies. The absence of the hPL^A morphology for $h > 3.0R_g$ should have the similar mechanism as that of the PL^A morphology, which has not been well explained before. The main reason is that the hC_{||}^A morphology can automatically adjust the domain shape in response to h . Specifically, at large h , the domain shape of hC_{||}^A deforms into lamella capped with a round end near the substrate (i.e., L'_⊥). In other words, the hC_{||}^A morphology can be regarded as a mixture of cylinders and lamellae. Therefore, it adapts to the variation of f and h better than hPL^A. Similarly, the phase boundary between the hS^A and hC_{||}^A morphologies shifts to small f and then back to large f as h increases due to the continuous change of the domain shape as well. Specifically, the domain curvature in the hS^A morphology first increases and then decreases when it changes from oblate to near sphere and then to perpendicular cylinder capped with a hemisphere (i.e., C_⊥^A).

To examine the effect of $\chi_{AB}N$ on the stability window of the hPL^A morphology, we construct the phase diagram with respect to f and $\chi_{AB}N$ for fixed $h = 1.6R_g$ in Figure 5a. The width of the window of hPL^A does not change notably as $\chi_{AB}N$ increases, but shifting to large f . The shift of the phase boundaries mainly results from the increasing order of the interfacial energy of the L_⊥, hPL^A, and hL_{||} morphologies. To investigate the influence of h and $\chi_{AB}N$ on the formation of hPL^A for ideally symmetric $f = 0.5$, we construct the corresponding phase diagram in Figure 5b. As $\chi_{AB}N$ increases, the stable window of hPL^A gradually narrows until it disappears at $\chi_{AB}N \approx 45$. This is because the A/B interfacial becomes increasingly dominant over the surface energy with increasing $\chi_{AB}N$ under the situation of unchanged surface preference, reducing the advantage of hPL^A over L_⊥ in the surface energy. In a word, the formation of hPL^A at $f = 0.5$ requires some specific conditions, especially ultrathin films with neutral-preferential surfaces.

The above results demonstrate that the surface preference of the substrate to B-block is a key factor of stabilizing the hPL^A morphology in ultrathin films. In experiments, the surface affinity of the substrate can be readily modified to regulate the self-assembly of block copolymers overlying it.^{30,33} To know how the preferential strength of the bottom surface affects the stable window of the hPL^A morphology with respect to h , we turn to construct the phase diagram with respect to h and $|\chi_w N| = \chi_{AW}N = -\chi_{BW}N$ for $f = 0.5$ and $\chi_{AB}N = 30$ (Figure 6). When the interaction strength $|\chi_w N|$ is lowered, the hPL^A region narrows rapidly and vanishes at $|\chi_w N| \approx 24$. In ultrathin films, the formation of the hL_{||} morphology is dominated by the surface energy (i.e., $|\chi_w N|$), while that of L_⊥ (or hC_{||}^A) is dominated by the interfacial energy (i.e., $\chi_{AB}N$). The formation of hPL^A

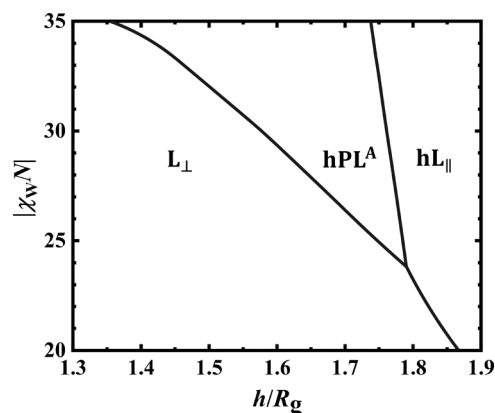


Figure 6. Phase diagram with respect to $|\chi_w N|$ and h for $f = 0.5$ and $\chi_{AB}N = 30$, where $\chi_{AW}N = |\chi_w N|$ and $\chi_{BW}N = -|\chi_w N|$.

between hL_{||} and hC_{||}^A is determined by the compromise between the interfacial energy and the surface energy. Therefore, the critical selectivity of the substrate for presence of the hPL^A morphology increases with $\chi_{AB}N$.

As previously reported, the phase separation of diblock copolymers in the films starts on the selective surface^{58,59} and leads to a tendency to form parallel morphologies. Accordingly, we utilize the DPD simulations to verify the formation of these structures in kinetics, especially hPL^A (Figure 7a). The estimated diagram is shown in Figure 7b. Although the chain models and the confinement models in the DPD and SCFT systems are quite different, a stable window of the hPL^A morphology is observed between L_⊥ and L_{||} in ultrathin films within $1.0R_g < h < 2.5R_g$. Moreover, the hPL^A region also shifts to small f as h increases, which is in qualitative agreement with the SCFT calculations. According to the phase diagrams in Figures 5 and 6, the shifting of the phase boundaries of hPL^A to smaller f and lower h in the phase diagram of DPD (Figure 7b) may be because the effective interaction parameter or the surface affinity are weaker than those in SCFT.

CONCLUSIONS

In summary, the self-assembly of AB diblock copolymers in ultrathin films with a neutral top surface and a B-selective substrate has been investigated by SCFT, focusing on the formation of a hexagonal dot pattern observed in experiments. Our SCFT results confirm that the stable hexagonal dot pattern can be formed by a symmetric AB diblock copolymer of $f = 0.5$, which is indeed a half-period perforated lamellar morphology

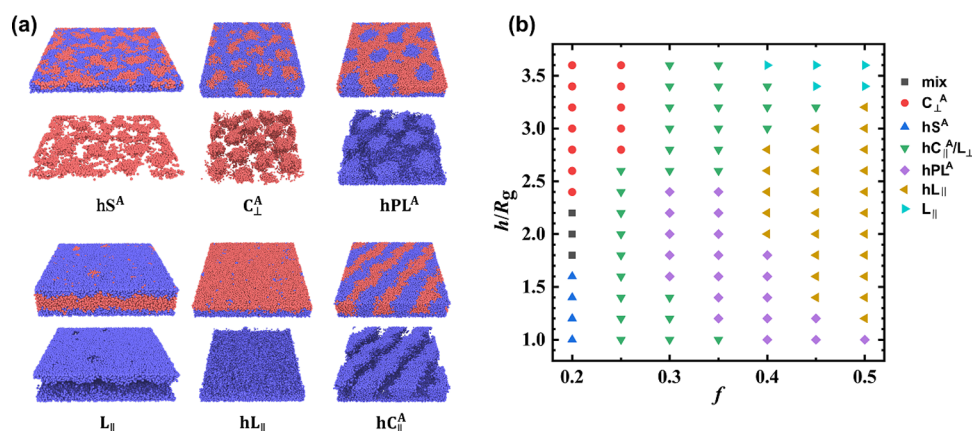


Figure 7. (a) Morphologies gained from DPD simulations. For each morphology, the upper plot contains both A- and B-particles while the lower plot contains only one type of particles to display the structure better. (b) Kinetic phase diagram by DPD simulation for $N_b = 40$ and $a_{AB} = 27.45$, where N_b denotes the total number of the beads in a single chain and a_{AB} the interaction parameter between A- and B-particles. The value of a_{AB} is calculated through the formula of $a_{AB} = 25 + 3.27 * \chi_{AB}N/N_b$.⁵⁷

(hPL^A). The hPL^A morphology is formed between a half-period parallel lamellar morphology (hL_{||}) and a half-period parallel cylinder morphology (hC_{||}^A) along decreasing thickness h . The transition is mainly to reduce the rapidly increasing A/B interfacial energy at the expense of surface energy. The phase diagram with respect to f and h demonstrates that the hPL^A phase region shifts to small f as h increases until it vanishes at a critical value of h . Its disappearance is mainly because the competing hC_{||}^A phase can continuously change shape to adapt to the increasing thickness.

We also examined the influence of $\chi_{AB}N$ on the stable region of hPL^A. Our results suggest that the hPL^A region with respect to h for $f = 0.5$ is gradually squeezed until disappearing by the hC_{||}^A region because the latter has more favorable interfacial energy than the former. Oppositely, increasing the preferential strength $|x_w N|$ of the bottom surface can widen the hPL^A window. In order to obtain hPL^A for high $\chi_{AB}N$, it is necessary to increase $|x_w N|$ accordingly. In addition, the hPL^A morphology is obtained in DPD simulations, confirming its kinetic stability. In brief, our work deepens the understanding of diblock copolymers in ultrathin films of asymmetric surface affinities.

■ ASSOCIATED CONTENT

SI Supporting Information

The Supporting Information is available free of charge at <https://pubs.acs.org/doi/10.1021/acs.macromol.3c00706>.

Self-consistent field theory (SCFT); and dissipative particle dynamics (DPD) (PDF)

■ AUTHOR INFORMATION

Corresponding Authors

Jiajia Zhou – South China Advanced Institute for Soft Matter Science and Technology, School of Molecular Science and Engineering and State Key Laboratory of Luminescent Materials and Devices, South China University of Technology, Guangzhou 510640, China; orcid.org/0000-0002-2258-6757; Email: zhouj2@scut.edu.cn

Weihua Li – State Key Laboratory of Molecular Engineering of Polymers, Key Laboratory of Computational Physical Sciences,

Department of Macromolecular Science, Fudan University, Shanghai 200433, China; orcid.org/0000-0002-5133-0267; Email: weihuali@fudan.edu.cn

Authors

Luyang Li – State Key Laboratory of Molecular Engineering of Polymers, Key Laboratory of Computational Physical Sciences, Department of Macromolecular Science, Fudan University, Shanghai 200433, China

Xiangmeng Jia – South China Advanced Institute for Soft Matter Science and Technology, School of Molecular Science and Engineering and State Key Laboratory of Luminescent Materials and Devices, South China University of Technology, Guangzhou 510640, China

Qingshu Dong – State Key Laboratory of Molecular Engineering of Polymers, Key Laboratory of Computational Physical Sciences, Department of Macromolecular Science, Fudan University, Shanghai 200433, China

Complete contact information is available at: <https://pubs.acs.org/10.1021/acs.macromol.3c00706>

Notes

The authors declare no competing financial interest.

■ ACKNOWLEDGMENTS

The authors thank Prof. Roy Shenhar for the helpful discussions. This work was supported by the National Natural Science Foundation of China (Grant Nos. 21925301 and 22203018).

■ REFERENCES

- (1) Bates, F. S.; Fredrickson, G. H. Block Copolymer Thermodynamics - Theory and Experiment. *Annu. Rev. Phys. Chem.* **1990**, *41*, 525–557.
- (2) Park, C.; Yoon, J.; Thomas, E. L. Enabling Nanotechnology with Self Assembled Block Copolymer Patterns. *Polymer* **2003**, *44*, 6725–6760.
- (3) Matsen, M. W. The Standard Gaussian Model for Block Copolymer Melts. *J. Phys. Condens. Matter* **2002**, *14*, R21–R47.
- (4) Urbas, A. M.; Maldovan, M.; DeRege, P.; Thomas, E. L. Bicontinuous Cubic Block Copolymer Photonic Crystals. *Adv. Mater.* **2002**, *14*, 1850–1853.
- (5) Maldovan, M.; Thomas, E. L. Diamond-Structured Photonic Crystals. *Nat. Mater.* **2004**, *3*, 593–600.

- (6) Mansky, P.; Liu, Y.; Huang, E.; Russell, T. P.; Hawker, C. J. Controlling Polymer-Surface Interactions with Random Copolymer Brushes. *Science* **1997**, *275*, 1458–1460.
- (7) Huang, C.; Zhu, Y.; Man, X. Block Copolymer Thin Films. *Phys. Rep.* **2021**, *932*, 1–36.
- (8) Crossland, E. J. W.; Kamperman, M.; Nedelcu, M.; Ducati, C.; Wiesner, U.; Smilgies, D.-M.; Toombes, G. E.; Hillmyer, M. A.; Ludwigs, S.; Steiner, U.; Henry, J. A Bicontinuous Double Gyroid Hybrid Solar Cell. *Nano Lett.* **2009**, *9*, 2807–2812.
- (9) Matsen, M. W.; Schick, M. Stable and Unstable Phases of a Diblock Copolymer Melt. *Phys. Rev. Lett.* **1994**, *72*, 2660–2663.
- (10) Bates, F. S. Polymer-Polymer Phase-Behavior. *Science* **1991**, *251*, 898–905.
- (11) Xie, N.; Li, W.; Qiu, F.; Shi, A.-C. σ Phase Formed in Conformationally Asymmetric AB-Type Block Copolymers. *ACS Macro Lett.* **2014**, *3*, 906–910.
- (12) Matsen, M. W.; Bates, F. S. Block Copolymer Microstructures in the Intermediate-Segregation Regime. *J. Chem. Phys.* **1997**, *106*, 2436–2448.
- (13) Matsen, M. W.; Bates, F. S. Unifying Weak- and Strong-Segregation Block Copolymer Theories. *Macromolecules* **1996**, *29*, 1091–1098.
- (14) Gottlieb, E. R.; Guliyeva, A.; Epps, T. H. From Lab to Fab: Enabling Enhanced Control of Block Polymer Thin-Film Nanostructures. *ACS Appl. Polym. Mater.* **2021**, *3*, 4288–4303.
- (15) Anastasiadis, S. H.; Russell, T.; Satija, S.; Majkrzak, C. Neutron Reflectivity Studies of the Surface-induced Ordering of Diblock Copolymer Films. *Phys. Rev. Lett.* **1989**, *62*, 1852–1855.
- (16) Matsen, M. W. Thin Films of Block Copolymer. *J. Chem. Phys.* **1997**, *106*, 7781–7791.
- (17) Koo, K.; Ahn, H.; Kim, S. W.; Ryu, D. Y.; Russell, T. P. Directed Self-Assembly of Block Copolymers in the Extreme: Guiding Microdomains from the Small to the Large. *Soft Matter* **2013**, *9*, 9059–9071.
- (18) Hu, H. Q.; Gopinadhan, M.; Osuji, C. O. Directed Self-Assembly of Block Copolymers: A Tutorial Review of Strategies for Enabling Nanotechnology with Soft Matter. *Soft Matter* **2014**, *10*, 3867–3889.
- (19) Ji, S. X.; Wan, L.; Liu, C. C.; Nealey, P. F. Directed Self-Assembly of Block Copolymers on Chemical Patterns: A Platform for Nanofabrication. *Prog. Polym. Sci.* **2016**, *54–55*, 76–127.
- (20) Liu, C. C.; Franke, E.; Mignot, Y.; Xie, R. L.; Yeung, C. W.; Zhang, J. Y.; Chi, C.; Zhang, C.; Farrell, R.; Lai, K. F.; Tsai, H.; Felix, N.; Corliss, D. Directed Self-Assembly of Block Copolymers for 7 Nanometre FinFET Technology and Beyond. *Nat. Electron.* **2018**, *1*, 562–569.
- (21) Yang, G. G.; Choi, H. J.; Han, K. H.; Kim, J. H.; Lee, C. W.; Jung, E. I.; Jin, H. M.; Kim, S. O. Block Copolymer Nanopatterning for Nonsemiconductor Device Applications. *ACS Appl. Mater. Interfaces* **2022**, *14*, 12011–12037.
- (22) Bates, F. S.; Schulz, M. F.; Khandpur, A. K.; Forster, S.; Rosedale, J. H.; Almdal, K.; Mortensen, K. Fluctuations, Conformational Asymmetry and Block-Copolymer Phase-Behavior. *Faraday Discuss.* **1994**, *98*, 7–18.
- (23) Takenaka, M.; Wakada, T.; Akasaka, S.; Nishitsuji, S.; Saijo, K.; Shimizu, H.; Kim, M. I.; Hasegawa, H. Orthorhombic Fddd Network in Diblock Copolymer Melts. *Macromolecules* **2007**, *40*, 4399–4402.
- (24) Lambooy, P.; Russell, T. P.; Kellogg, G. J.; Mayes, A. M.; Gallagher, P. D.; Satija, S. K. Observed Frustration in Confined Block-Copolymers. *Phys. Rev. Lett.* **1994**, *72*, 2899–2902.
- (25) Huang, E.; Rockford, L.; Russell, T. P.; Hawker, C. J. Nanodomain Control in Copolymer Thin Films. *Nature* **1998**, *395*, 757–758.
- (26) Li, W.; Liu, M.; Qiu, F.; Shi, A.-C. Phase Diagram of Diblock Copolymers Confined in Thin Films. *J. Phys. Chem. B* **2013**, *117*, 5280–5288.
- (27) Koneripalli, N.; Levicky, R.; Bates, F. S.; Ankner, J.; Kaiser, H.; Satija, S. K. Confinement-Induced Morphological Changes in Diblock Copolymer Films. *Langmuir* **1996**, *12*, 6681–6690.
- (28) Kellogg, G. J.; Walton, D. G.; Mayes, A. M.; Lambooy, P.; Russell, T. P.; Gallagher, P. D.; Satija, S. K. Observed Surface Energy Effects in Confined Diblock Copolymers. *Phys. Rev. Lett.* **1996**, *76*, 2503–2506.
- (29) Knoll, A.; Horvat, A.; Lyakhova, K. S.; Krausch, G.; Sevinck, G. J. A.; Zvelindovsky, A. V.; Magerle, R. Phase Behavior in Thin Films of Cylinder-Forming Block Copolymers. *Phys. Rev. Lett.* **2002**, *89*, No. 035501.
- (30) Kim, S.; Bates, C. M.; Thio, A.; Cushen, J. D.; Ellison, C. J.; Willson, C. G.; Bates, F. S. Consequences of Surface Neutralization in Diblock Copolymer Thin Films. *ACS Nano* **2013**, *7*, 9905–9919.
- (31) Durand, W. J.; Carlson, M. C.; Maher, M. J.; Blachut, G.; Santos, L. J.; Tein, S.; Ganesan, V.; Ellison, C. J.; Willson, C. G. Experimental and Modeling Study of Domain Orientation in Confined Block Copolymer Thin Films. *Macromolecules* **2016**, *49*, 308–316.
- (32) Walton, D. G.; Kellogg, G. J.; Mayes, A. M.; Lambooy, P.; Russell, T. P. A Free-Energy Model for Confined Diblock Copolymers. *Macromolecules* **1994**, *27*, 6225–6228.
- (33) Maher, M. J.; Bates, C. M.; Blachut, G.; Sirard, S.; Self, J. L.; Carlson, M. C.; Dean, L. M.; Cushen, J. D.; Durand, W. J.; Hayes, C. O.; Ellison, C. J.; Willson, C. G. Interfacial Design for Block Copolymer Thin Films. *Chem. Mater.* **2014**, *26*, 1471–1479.
- (34) Shull, K. R. Mean-Field Theory of Block Copolymers-Bulk Melts, Surfaces, and Thin-Films. *Macromolecules* **1992**, *25*, 2122–2133.
- (35) Turner, M. S. Equilibrium Properties of a Diblock Copolymer Lamellar Phase Confined between Flat Plates. *Phys. Rev. Lett.* **1992**, *69*, 1788–1791.
- (36) Sikka, M.; Singh, N.; Karim, A.; Bates, F. S.; Satija, S. K.; Majkrzak, C. F. Entropy-Driven Surface Segregation in Block Copolymer Melts. *Phys. Rev. Lett.* **1993**, *70*, 307–310.
- (37) Albert, J. N. L.; Epps, I. T. H. Self-Assembly of Block Copolymer Thin Films. *Mater. Today* **2010**, *13*, 24–33.
- (38) Coulon, G.; Collin, B.; Ausserre, D.; Chatenay, D.; Russell, T. P. Islands and Holes on the Free-Surface of Thin Diblock Copolymer Films. 1. Characteristics of Formation and Growth. *J. Phys.* **1990**, *51*, 2801–2811.
- (39) Morkved, T. L.; Jaeger, H. M. Thickness-Induced Morphology Changes in Lamellar Diblock Copolymer Ultrathin Films. *Europhys. Lett.* **1997**, *40*, 643–648.
- (40) Fasolka, M. J.; Mayes, A. M. Block Copolymer Thin Films: Physics and Applications. *Annu. Rev. Mater. Res.* **2001**, *31*, 323–355.
- (41) Tang, W. H. Confinement of Symmetric Diblock Copolymer Thin Films. *Macromolecules* **2000**, *33*, 1370–1384.
- (42) Meng, D.; Wang, Q. A. Complex Morphologies in Thin Films of Symmetric Diblock Copolymers as Stable and Unstable Phases. *Soft Matter* **2010**, *6*, 5891–5906.
- (43) Peters, R. D.; Stasiak, P.; Matsen, M. W.; Dalnoki-Veress, K. Morphology Induced Spinodal Decomposition at the Surface of Symmetric Diblock Copolymer Films. *ACS Macro Lett.* **2013**, *2*, 441–445.
- (44) Kim, Y.; Yong, D.; Lee, W.; Ahn, H.; Kim, J. H.; Kim, J. U.; Ryu, D. Y. Order-to-Disorder Transition of Lamella-Forming PS-*b*-P2VP Films Confined between the Preferential Surface and Neutral Substrate. *Macromolecules* **2019**, *52*, 8672–8681.
- (45) Michman, E.; Langenberg, M.; Stenger, R.; Oded, M.; Schwartzman, M.; Muller, M.; Shenhar, R. Controlled Spacing between Nanopatterned Regions in Block Copolymer Films Obtained by Utilizing Substrate Topography for Local Film Thickness Differentiation. *ACS Appl. Mater. Interfaces* **2019**, *11*, 35247–35254.
- (46) Michman, E.; Oded, M.; Shenhar, R. Dual Block Copolymer Morphologies in Ultrathin Films on Topographic Substrates: The Effect of Film Curvature. *Polymers* **2022**, *14*, No. 2377.
- (47) Michman, E.; Oded, M.; Shenhar, R. Non-Bulk Morphologies of Extremely Thin Block Copolymer Films Cast on Topographically Defined Substrates Featuring Deep Trenches: The Importance of Lateral Confinement. *Polymers* **2023**, *15*, No. 1035.
- (48) Mansky, P.; Russell, T. P.; Hawker, C. J.; Pitsikalis, M.; Mays, J. Ordered Diblock Copolymer Films on Random Copolymer Brushes. *Macromolecules* **1997**, *30*, 6810–6813.

- (49) Fasolka, M. J.; Banerjee, P.; Mayes, A. M.; Pickett, G.; Balazs, A. C. Morphology of Ultrathin Supported Diblock Copolymer Films: Theory and Experiment. *Macromolecules* **2000**, *33*, 5702–5712.
- (50) Khanna, V.; Cochran, E. W.; Hexemer, A.; Stein, G. E.; Fredrickson, G. H.; Kramer, E. J.; Li, X.; Wang, J.; Hahn, S. F. Effect of Chain Architecture and Surface Energies on the Ordering Behavior of Lamellar and Cylinder Forming Block Copolymers. *Macromolecules* **2006**, *39*, 9346–9356.
- (51) Yu, N.; Polycarpou, A. A. Adhesive Contact Based on the Lennard–Jones Potential: A Correction to the Value of the Equilibrium Distance as Used in The Potential. *J. Colloid Interface Sci.* **2004**, *278*, 428–435.
- (52) Anderson, J. A.; Lorenz, C. D.; Travesset, A. General Purpose Molecular Dynamics Simulations Fully Implemented on Graphics Processing Units. *J. Comput. Phys.* **2008**, *227*, 5342–5359.
- (53) O’Driscoll, B. M. D.; Griffiths, G. H.; Matsen, M. W.; Perrier, S.; Ladmiral, V.; Hamley, I. W. Lateral Phase Separation in Grafted Diblock Copolymer Films. *Macromolecules* **2010**, *43*, 8177–8184.
- (54) Shi, A.-C.; Li, B. Self-Assembly of Diblock Copolymers under Confinement. *Soft Matter* **2013**, *9*, 1398–1413.
- (55) Matsen, M. W.; Griffiths, G. H. Melt Brushes of Diblock Copolymer. *Eur. Phys. J. E* **2009**, *29*, 219–227.
- (56) Pereira, G. G.; Williams, D. R. M. Thin Films of Perpendicularly Oriented Diblock Copolymers: Lamellar Distortions Driven by Surface-Diblock Interfacial Tensions. *Macromolecules* **1999**, *32*, 1661–1664.
- (57) Groot, R. D.; Warren, P. B. Dissipative Particle Dynamics: Bridging the Gap Between Atomistic and Mesoscopic Simulation. *J. Chem. Phys.* **1997**, *107*, 4423–4435.
- (58) Peters, R. D.; Dalnoki-Veress, K. Film Thickness Dependent Ordering Dynamics of Lamellar Forming Diblock Copolymer Thin Films. *Eur. Phys. J. E* **2012**, *35*, No. 132.
- (59) Weith, V.; Krekhov, A.; Zimmermann, W. Stability and Orientation of Lamellae in Diblock Copolymer Films. *J. Chem. Phys.* **2013**, *139*, No. 054908.

Supporting Information:

Thickness-Controlled Phase Transitions of AB Diblock Copolymers in Asymmetric Ultrathin Films

Luyang Li,[†] Xiangmeng Jia,[‡] Qingshu Dong,[†] Jiajia Zhou,^{*,‡} and Weihua Li^{*,†}

[†]*State Key Laboratory of Molecular Engineering of Polymers, Key Laboratory of Computational Physical Sciences, Department of Macromolecular Science, Fudan University, Shanghai 200433, China*

[‡]*South China Advanced Institute for Soft Matter Science and Technology, School of Molecular Science and Engineering and State Key Laboratory of Luminescent Materials and Devices, South China University of Technology, Guangzhou 510640, China*

E-mail: zhouj2@scut.edu.cn; weihuali@fudan.edu.cn

This PDF file includes:

Self-consistent field theory (SCFT),

Dissipative particle dynamics (DPD).

Self-consistent field theory (SCFT)

The quantity Q is the partition function of a single copolymer chain interacting with their mean fields, determined by

$$Q = \frac{1}{V} \int d\mathbf{r} q_{\mathbf{K}}(\mathbf{r}, s) q_{\mathbf{K}}^{\dagger}(\mathbf{r}, s) \quad (1)$$

Here $q_{\mathbf{K}}(\mathbf{r}, s)$ and $q_{\mathbf{K}}^{\dagger}(\mathbf{r}, s)$ ($\mathbf{K} = \text{A and B}$) are two sets of conjugate propagator functions of \mathbf{K} -block starting from two distinguishable ends at $s = 0$ and $s = 1$, satisfying the following modified diffusion equations

$$\frac{\partial q_{\mathbf{K}}(\mathbf{r}, s)}{\partial s} = \nabla^2 q_{\mathbf{K}}(\mathbf{r}, s) - w_{\mathbf{K}}(\mathbf{r}) q_{\mathbf{K}}(\mathbf{r}, s) \quad (2)$$

$$-\frac{\partial q_{\mathbf{K}}^{\dagger}(\mathbf{r}, s)}{\partial s} = \nabla^2 q_{\mathbf{K}}^{\dagger}(\mathbf{r}, s) - w_{\mathbf{K}}(\mathbf{r}) q_{\mathbf{K}}^{\dagger}(\mathbf{r}, s) \quad (3)$$

Minimization of the free energy with respect to $\phi_{\mathbf{A}}(\mathbf{r})$, $\phi_{\mathbf{B}}(\mathbf{r})$, $\omega_{\mathbf{A}}(\mathbf{r})$ and $\omega_{\mathbf{B}}(\mathbf{r})$ leads to the following SCFT equations

$$w_{\mathbf{A}}(\mathbf{r}) = \chi_{\text{AB}} N \phi_{\mathbf{B}}(\mathbf{r}) + \chi_{\text{AW}} N \phi_{\mathbf{W}}(\mathbf{r}) + \chi_{\text{AT}} N \phi_{\mathbf{T}}(\mathbf{r}) + \xi(\mathbf{r}) \quad (4)$$

$$w_{\mathbf{B}}(\mathbf{r}) = \chi_{\text{AB}} N \phi_{\mathbf{A}}(\mathbf{r}) + \chi_{\text{BW}} N \phi_{\mathbf{W}}(\mathbf{r}) + \chi_{\text{BT}} N \phi_{\mathbf{T}}(\mathbf{r}) + \xi(\mathbf{r}) \quad (5)$$

$$\phi_{\mathbf{A}}(\mathbf{r}) = \frac{1}{Q} \int_0^f ds q_{\mathbf{A}}(\mathbf{r}, s) q_{\mathbf{A}}^{\dagger}(\mathbf{r}, s) \quad (6)$$

$$\phi_{\mathbf{B}}(\mathbf{r}) = \frac{1}{Q} \int_f^1 ds q_{\mathbf{B}}(\mathbf{r}, s) q_{\mathbf{B}}^{\dagger}(\mathbf{r}, s) \quad (7)$$

The free energy are divided into A/B interaction energy (U_{AB}), surface interaction energy

(U_{Surf}), and entropic contribution ($(-TS)$) as:

$$\frac{U_{\text{AB}}}{nk_B T_0} = \frac{1}{V} \int d\mathbf{r} \chi_{\text{AB}} N \phi_{\text{A}}(\mathbf{r}) \phi_{\text{B}}(\mathbf{r}), \quad (8)$$

$$\begin{aligned} \frac{U_{\text{Surf}}}{nk_B T_0} &= \frac{1}{V} \int d\mathbf{r} \{ \chi_{\text{AW}} N \phi_{\text{A}}(\mathbf{r}) \phi_{\text{W}}(\mathbf{r}) + \chi_{\text{BW}} N \phi_{\text{B}}(\mathbf{r}) \phi_{\text{W}}(\mathbf{r}) \\ &\quad + \chi_{\text{AT}} N \phi_{\text{A}}(\mathbf{r}) \phi_{\text{T}}(\mathbf{r}) + \chi_{\text{BT}} N \phi_{\text{B}}(\mathbf{r}) \phi_{\text{T}}(\mathbf{r}) \}, \end{aligned} \quad (9)$$

$$-TS = F - U_{\text{AB}} - U_{\text{Surf}}. \quad (10)$$

We use the pseudo-spectral method^{S1-S3} to solve the modified diffusion equations and implement the Anderson mixing iteration scheme^{S4} to accelerate the converging speed toward SCFT solutions. To ensure reliable accuracy, the chain contour is divided into 100 points, i.e., $\Delta s = 10^{-2}$, and the lattice grids of the computational box $N_x \times N_y \times N_z$ are chosen as $64 \times 64 \times 64$ to make the maximal lattice spacings Δx , Δy , and Δz smaller than $0.15R_g$.

Dissipative Particle Dynamics (DPD)

DPD simulations are performed in the NVT canonical ensemble. The time evolution of DPD beads with unit mass is governed by Newton's equations of motion:^{S5}

$$\frac{d\mathbf{r}_i}{dt} = \mathbf{v}_i, \quad \frac{d\mathbf{v}_i}{dt} = \mathbf{f}_i \quad (11)$$

where

$$\mathbf{f}_i = \sum_{j \neq i} (\mathbf{F}_{ij}^{\text{C}} + \mathbf{F}_{ij}^{\text{D}} + \mathbf{F}_{ij}^{\text{R}}) \quad (12)$$

The force acting on each bead consists of conservative $\mathbf{F}_{ij}^{\text{C}}$, dissipative $\mathbf{F}_{ij}^{\text{D}}$, and random $\mathbf{F}_{ij}^{\text{R}}$ force. Each part is pairwise-additive, repulsive and short-range with a cutoff at $r = 1.0$. The conservative

force \mathbf{F}_{ij}^C is a soft-repulsive interaction acting between two adjacent beads:

$$\mathbf{F}_{ij}^C = \begin{cases} a_{ij}(1-r_{ij})\hat{\mathbf{r}}_{ij} & (r_{ij} < 1) \\ 0 & (r_{ij} \geq 1) \end{cases} \quad (13)$$

where r_{ij} denotes the distance between the centers of beads i and j with $\mathbf{r}_{ij} = \mathbf{r}_i - \mathbf{r}_j$, $r_{ij} = |\mathbf{r}_{ij}|$ and $\hat{\mathbf{r}}_{ij} = \mathbf{r}_{ij}/|\mathbf{r}_{ij}|$. The interaction parameter a_{ij} is related to the Flory-Huggins χ -parameter by $a_{ij} = 25 + 3.27\chi_{ij}$ for a fixed number density $\rho = 3$,^{S5} which implies $a_{ii} = 25$ for the interaction between the beads of the same type. In our simulation, 40 beads are used to represent a single chain and $a_{AB} = 27.45$ is chosen, corresponding to $\chi N \approx 30$.

The dissipative force \mathbf{F}_{ij}^D and the random force \mathbf{F}_{ij}^R take the form:

$$\mathbf{F}_{ij}^D = -\gamma w^D(r_{ij})(\hat{\mathbf{r}}_{ij} \cdot \mathbf{v}_{ij})\hat{\mathbf{r}}_{ij} \quad (14)$$

$$\mathbf{F}_{ij}^R = \sigma w^R(r_{ij})\theta_{ij}\hat{\mathbf{r}}_{ij} \quad (15)$$

where $\mathbf{v}_{ij} = \mathbf{v}_i - \mathbf{v}_j$ is the relative velocity, γ is the friction coefficient and σ is the noise level controlling the intensity of the random force and is set to be 3.^{S5} $\theta_{ij}(t)$ is a randomly fluctuating variable with zero mean and unit variance, satisfying Gaussian statistics:

$$\langle \theta_{ij}(t) \rangle = 0, \quad (16)$$

$$\langle \theta_{ij}(t)\theta_{kl}(t') \rangle = (\delta_{ik}\delta_{jl} + \delta_{il}\delta_{jk})\delta(t-t') \quad (17)$$

where δ represents the Dirac Delta function. The random force is related to the dissipative force so that they satisfy the fluctuation-dissipation relation:^{S6} $\sigma^2 = 2\gamma k_B T$. The weight function w^D and w^R provide the range of interaction for DPD particles with a common choice:

$$w^D(r) = [w^R(r)]^2 = \begin{cases} (1-r)^2, & (r < 1) \\ 0, & (r \geq 1) \end{cases} \quad (18)$$

The combined effect of these two forces is that of a thermostat, ensuring that the simulation is performed in a canonical ensemble. Each pair of beads on the polymeric chain is connected by a harmonic spring potential as: $V_{\text{bond}}(r) = \frac{1}{2}k_b(r - r_b)^2$, where r_b is the reference length, r is the distance between the beads and k_b is the spring constant.^{S7} The two constants are set as $r_b = 0$ and $k_b = 4$ for the conventional blocks.

References

- (S1) Rasmussen, K.; Kalosakas, G. Improved Numerical Algorithm for Exploring Block Copolymer Mesophases. *J. Polym. Sci. B: Polym. Phys.* **2002**, *40*, 1777–1783.
- (S2) Stasiak, P.; Matsen, M. W. Efficiency of Pseudo-Spectral Algorithms with Anderson Mixing for the SCFT of Periodic Block-Copolymer Phases. *Eur. Phys. J. E: Soft Matter* **2011**, *34*, 110.
- (S3) Tzeremes, G.; Rasmussen, K. K.; Lookman, T.; Saxena, A. Efficient Computation of the Structural Phase Behavior of Block Copolymers. *Phys. Rev. E: Stat. Phys., Plasmas, Fluids, Relat. Interdiscip. Top.* **2002**, *65*, 041806.
- (S4) Thompson, R. B.; Rasmussen, K. O.; Lookman, T. Improved Convergence in Block Copolymer Self-Consistent Field Theory by Anderson Mixing. *J. Chem. Phys.* **2004**, *120*, 31–4.
- (S5) Groot, R. D.; Warren, P. B. Dissipative Particle Dynamics: Bridging the Gap Between Atomistic and Mesoscopic Simulation. *J. Chem. Phys.* **1997**, *107*, 4423–4435.
- (S6) Espanol, P.; Warren, P. Statistical Mechanics of Dissipative Particle Dynamics. *Europhys. Lett.* **1995**, *30*, 191.
- (S7) Groot, R. D.; Madden, T. J. Dynamic Simulation of Diblock Copolymer Microphase Separation. *J. Chem. Phys.* **1998**, *108*, 8713–8724.